CHEMISTRY OF MATERIALS
Article

Chem. Mater. **2011,** *23,* 293–300 293
DOI:10.1021/cm102922q

Iron and Manganese Pyrophosphates as Cathodes for Lithium-Ion Batteries

Hui Zhou,[†] Shailesh Upreti,[†] Natasha A. Chernova,[†] Geoffroy Hautier,[‡] Gerbrand Ceder,[‡] and M. Stanley Whittingham*,[†]

[†]*Materials Science and Engineering, State University of New York at Binghamton, Binghamton, New York 13902-6000, United States, and* [‡]*Department of Materials Science and Engineering, Massachusetts Institute of Technology, Cambridge, Massachusetts 02139, United States*

Received October 11, 2010. Revised Manuscript Received December 1, 2010

The mixed-metal phases, ($Li_2Mn_{1-y}Fe_yP_2O_7$, $0 \le y \le 1$), were synthesized using a "wet method", and found to form a solid solution in the $P2_1/a$ space group. Both thermogravimetric analysis and magnetic susceptibility measurements confirm the 2+ oxidation state for both the Mn and Fe. The electrochemical capacity improves as the Fe concentration increases, as do the intensities of the redox peaks of the cyclic voltammogram, indicating higher lithium-ion diffusivity in the iron phase. The two Li^+ ions in the three-dimensional tunnel structure of the pyrophosphate phase allows for the cycling of more than one lithium per redox center. Cyclic voltammograms show a second oxidation peak at ~5 V and ~5.3 V, indicative of the extraction of the second lithium ion, in agreement with ab initio computation predictions. Thus, electrochemical capacities exceeding 200 Ah/kg may be achieved if a stable electrolyte is found.

Introduction

Since the commercialization of lithium-ion batteries in the 1990s,[1] they have undergone intensive scientific research and successful applications in a variety of portable electronic devices. The oxide-based materials—$LiCoO_2$, $LiNiO_2$, and the spinel $LiMn_2O_4$—and all their substituted variations have been extensively studied as positive electrode materials.[2−4] The report on the olivine $LiFePO_4$ caused a paradigm shift for cathode materials from oxides to polyanionic compounds.[5] In the past decade, three-dimensional (3D) framework cathodes with XO_4 polyanions, especially PO_4, have attracted considerable attention, because of the inductive effect from polyanionic groups that leads to a higher operating voltage than that in oxides.[6] Also, a 3D framework offers the practical advantage of increased stability and, hence, safety.[7,8] Nonetheless, the main drawbacks of these compounds are their poor electronic and ionic conductivity and their relatively low volumetric capacity. The former has been successfully overcome through carbon coating, nanosizing, and partial substitution, permitting $LiFePO_4$ to break into the commercial market successfully.[9−12]

However, the low volumetric energy density of $LiFePO_4$ precludes it from use in space-restrictive applications. One may overcome the density barrier by increasing the number of lithium ions cycled per redox center above unity. There are several materials already known to react with more than one lithium per redox center: VSe_2, V_2O_5, $Li_xNi_{0.5}Mn_{0.5}O_2$ and $VOPO_4$, etc.[13−18] However, each of them has its own challenge, including that of not providing a source of lithium to be cycled. Thus, a search is underway for lithium-containing compounds that preferably contain stable polyanions.

Recently, a new pyrophosphate, $Li_2MnP_2O_7$, has been reported;[19] it has a 3D framework composed of MnO_5 square pyramids sharing edges with MnO_6 octahedra, which are further interconnected through P_2O_7 groups

*Author to whom correspondence should be addressed. Tel.: (607) 777-4623. Fax: (607) 777-4623. E-mail: stanwhit@gmail.com.

(1) Nagaura, T.; Tozawa, K. *Prog. Batteries Solar Cells* **1990**, *9*, 209.
(2) Mizushima, K.; Jones, P. C.; Wiseman, P. J.; Goodenough, J. B. *Mater. Res. Bull.* **1980**, *15*, 783.
(3) Thackeray, M. M.; David, W. I. F.; Bruce, P. G.; Goodenough, J. B. *Mater. Res. Bull.* **1983**, *18*, 461.
(4) Dahn, J. R.; Sacken, U.; von; Juzkow, M. W.; Al-Janaby, H. *J. Electrochem. Soc.* **1991**, *138*, 2207.
(5) Padhi, A. K.; Nanjundaswamy, K. S.; Goodenough, J. B. *J. Electrochem. Soc.* **1997**, *144*, 1188. Padhi, A. K.; Nanjundaswamy, K. S.; Masquelier, C.; Goodenough, J. B. *J. Electrochem. Soc.* **1997**, *144*, 2581.
(6) Padhi, A. K.; Nanjundaswamy, K. S.; Masquelier, C.; Okada, S.; Goodenough, J. B. *J. Electrochem. Soc.* **1997**, *144*, 1609.
(7) Tarascon, J. -M.; Armand, M. *Nature* **2001**, *414*, 359.
(8) Goodenough, J. B. *J. Power Sources* **2007**, *174*, 996.
(9) Yamada, A.; Chung, S. C.; Hinokuma, K. J. *J. Electrochem. Soc.* **2001**, *148*, A224.
(10) Chung, S. Y.; Bloking, J. T.; Chiang, Y. M. *Nat. Mater.* **2002**, *1*, 123.
(11) Ellis, B.; Kan, W. H.; Makahnouk, W. R. M.; Nazar, L. F. *J. Mater. Chem.* **2007**, *17*, 3248.
(12) Hong, J.; Wang, C. S.; Chen, X.; Upreti, S.; Whittingham, M. S. *Electrochem. Solid-State Lett.* **2009**, *12*, A33.
(13) Whittingham, M. S. *Chem. Rev.* **2004**, *104*, 4271.
(14) Whittingham, M. S. *Mater. Res. Bull.* **1978**, *13*, 959.
(15) Delmas, C.; Cognac-Auradou, H.; Cocciantelli, J. M.; Ménétrier, M.; Doumerc, J. P. *Solid State Ionics* **1994**, *69*, 257.
(16) Yang, X.-Q.; McBreen, J.; Yoon, W.-S.; Grey, C. P. *Electrochem. Commun.* **2002**, *4*, 649.
(17) Song, Y.; Zavalij, P. Y.; Whittingham, M. S. *J. Electrochem. Soc.* **2005**, *152*, A721.
(18) Ban, C.; Chernova, N. A.; Whittingham, M. S. *Electrochem. Commun.* **2009**, *11*, 522.
(19) Adam, L.; Guesdon, A.; Raveau, B. *J. Solid State Chem.* **2008**, *181*, 3110.

Published on Web 12/21/2010

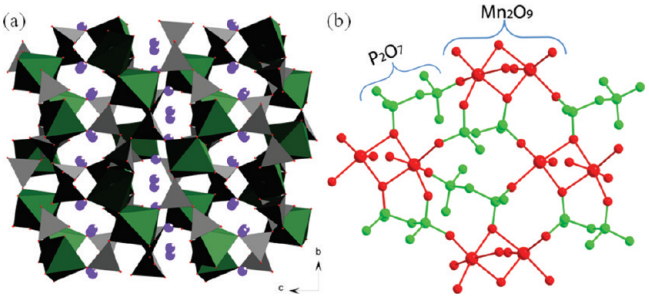

Figure 1. (a) Polyhedral representation of the 3D structure of $Li_2MnP_2O_7$ along [100] and (b) depiction of the connectivity between Mn_2O_9 with P_2O_7 units in the *ab* plane.

(see Figure 1). There are two lithium ions located in the tunnels along [100], which suggests that they might be mobile and removable. Lithium pyrophosphates $LiMP_2O_7$ (M = Fe, V) have also been studied recently,[20−23] mainly for their interesting crystal chemistry. They are less appealing for battery applications, because of their lower theoretical capacities: 113 mAh/g for $LiFeP_2O_7$ and 117 mAh/g for $LiVP_2O_7$. Here, we report the synthesis and the detailed structural, electrochemical, and magnetic characterization of the $Li_2Mn_{1-y}Fe_yP_2O_7$ solid solution with $y = 0$, 0.2, 0.5, 0.8, and 1.

Experimental Section

All the samples were synthesized through a "wet" method based on mixing stoichiometric aqueous solutions of precursors followed by thermal treatments. The general procedure involves the mixing of soluble precursors in distilled water, followed by a slow evaporation through continuous stirring to dryness before annealing the resultant solids.[24] The precursors for the synthesis of $Li_2Mn_{1-y}Fe_yP_2O_7$ were $Li(CH_3COO)$, $Fe(CH_3COO)_2$, $Mn(CH_3COO)_2$, and $NH_4H_2PO_4$ dissolved in 100 mL of distilled water to give a 0.02 M lithium solution. The self-adjusted pH values of all of the solutions were determined to be ~4.5−5. The solutions were stirred and evaporated on a hot plate in the hood, followed by vacuum oven overnight drying at 90 °C. Finally, the solids were annealed in a H_2/He atmosphere at temperatures ranging from 400 °C to 700 °C with intermediate grinding.

The structure of the samples was characterized by powder X-ray diffraction (XRD), using a Scintag Model XDS2000 $\theta-\theta$ powder diffractometer that was equipped with a Ge(Li) solid-state detector and Cu Kα sealed tube ($\lambda = 1.54178$ Å). Data were collected over the range of 5°−90° 2θ with a step size of 0.02° and exposure time of 10 s; the samples were rotated to diminish the effects of possible preferred orientation. High-resolution synchrotron powder XRD data were collected using Beamline 11-BM at the Advanced Photon Source (APS), Argonne National Laboratory, using an average wavelength of 0.413612 Å. Discrete detectors covering an angular range from −6° 2θ to 28° 2θ are scanned over a 2θ range of 34°, with data points collected in 2θ steps of every 0.001° and at a rate of 0.1°/s. The Rietveld refinement of the powder XRD patterns was done using the GSAS/EXPGUI package.[25,26] The morphology and particle size were characterized by scanning electron microscopy (SEM), using a ZeissSupra-55 field emission scanning electron microscope at 30 kV. Thermogravimetric analysis (TGA) was performed on a Perkin−Elmer Model TGA7 system under an O_2 atmosphere with a heating rate of 5 °C/min, to determine the ferrous content. The infrared spectra were recorded using KBr pellets between 400 cm^{-1} and 4000 cm^{-1}, using a Perkin−Elmer Model 1600 FTIR instrument.

The magnetic properties were studied using a Quantum Design MPMS XL SQUID magnetometer. The dc susceptibility was measured in a magnetic field of 1000 Oe upon cooling the samples from 350 K to 2 K. Field-cooled (FC) and zero-field-cooled (ZFC) curves were measured at 10 Oe between 2 K and 300 K. Before taking ZFC data, the remnant field was quenched to < 3 mOe, using the low-field option and the sample was cooled in zero field to 2 K. After that, the 10 Oe field was applied and the ZFC data were acquired while heating the sample up to 300 K, followed by FC data acquisition in the same field upon cooling.

The electrochemical properties of these samples were evaluated in 2325-type coin cells, using a VMP multichannel potentiostat (Biologic) with pure lithium foil (Aldrich, thickness of 0.38 mm) as the anode. The cathode was prepared by mixing each sample with Acetylene Black and poly(tetrafluoroethylene) powder in a weight ratio of 80:10:10. After the poweder mixture was ground in a mortar for ~30 min, they were hot-pressed into a stainless Exmet grid at a pressure of 5 tons and a temperature of 150 °C for 30 min with a typical loading of 35−40 mg/cm^2. The electrolyte was 1 M $LiPF_6$ (lithium hexafluorophosphate) dissolved in a mixture solution of ethylene carbonate (EC) and dimethyl carbonate (DMC) (LP30 from EM Industries) in a volume ratio of 1:1; a Celgard 2400 separator (Hoechst Celaese) was used. The assembling of the coin cells were done in a glovebox filled with pure helium. The cycling was performed between 1.5 V and 4.8 V, with a current density of 0.1 mA/cm^2 at room temperature.

Ab initio computations were performed in the density functional theory (DFT) framework, using the generalized gradient approximation functional parametrized by Perdew, Burke, and Ernzerhof (PBE) with Hubbard U corrections (GGA+U).[27,28] U values of 3.9 and 4.0 eV were respectively used on the *d*-states of Mn and Fe, as determined from the experimental oxidation energies.[29] All calculations were performed with the Vienna Ab Initio Simulation Package (VASP) with the provided projector augmented wave (PAW) pseudopotentials.[30,31] All computations were run assuming a ferromagnetic state and with an energy cutoff of 520 eV. A *k*-point density of at least 500/(number of atoms in unit cell) *k*-points was used for all the Brillouin integrations.

To determine the computed voltage profile along the $Li_2MP_2O_7$−MP_2O_7 line, several orderings were enumerated at the $Li_xMP_2O_7$ ($x = 1.75$, 1.5, 1.25, 1.0, 0.75, 0.5, 0.25, and 0.0) compositions, using an algorithm described by Hart et al.[32] For each of those compositions, 20 orderings with the lowest electrostatic

(20) Rousse, G.; Wurm, C.; Morcrette, M.; Rodriguez-Carvajal, J.; Gaubicher, J.; Masquelier, C. *Int. J. Inorg. Mater.* **2001**, *3*, 881.
(21) Uebou, Y.; Okada, S.; Egashira, M.; Yamaki, J. *Solid State Ionics* **2002**, *148*, 323.
(22) Salah, A.; Jozwiak, P.; Garbarczyk, J.; Benkhouja, K.; Zaghib, K.; Gendron, F.; Julien, C. M. *J. Power Sources* **2005**, *140*, 370.
(23) Barker, J.; Gover, R. K. B.; Burns, P.; Bryan, A. *Electrochem. Solid-State Lett.* **2005**, *8*, A446.
(24) Belkouch, J.; Monceaux, L.; Bordes, E.; Courtine, P. *Mater. Res. Bull.* **1995**, *30*, 149.
(25) Toby, B. H. *J. Appl. Crystallogr.* **2001**, *34*, 210.
(26) Larson, A. C.; VonDreele, R. B. General Structure Analysis System (GSAS). Los Alamos Natl. Lab., [Rep.] LA (U.S.) **2000**, *86*, 748.
(27) Dudarev, S. L.; Savrasov, S. Y.; Humphreys, C. J.; Sutton, A. P. *Phys. Rev. B* **1998**, *57*, 1505.
(28) Perdew, J.; Burke, K.; Ernzerhof, M. *Phys. Rev. Lett.* **1996**, *77*, 3865.
(29) Wang, L.; Maxisch, T.; Ceder, G. *Phys. Rev. B* **2006**, *73*, 195107.
(30) Kresse, G.; Furthmuller, J. *Comput. Mater. Sci.* **1996**, *6*, 15.
(31) Blöchl, P. *Phys. Rev. B* **1994**, *50*, 17953.
(32) Hart, G. L.; Forcade, R. W. *Phys. Rev. B* **2008**, *77*, 1.

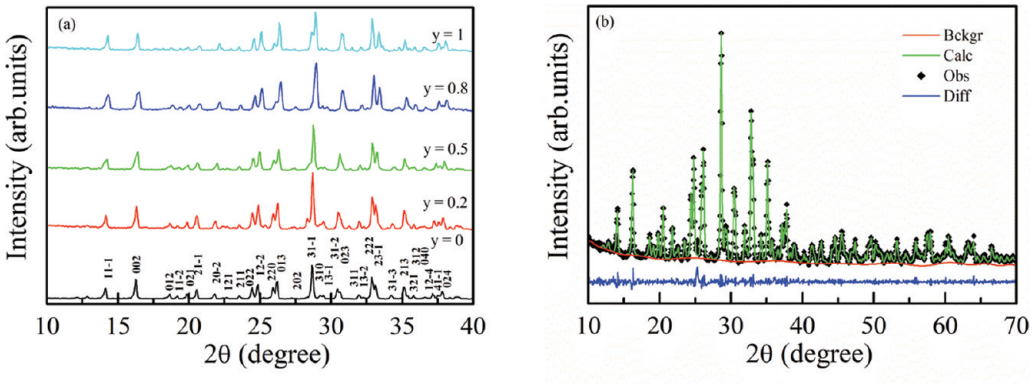

Figure 2. (a) X-ray diffraction (XRD) patterns of the $Li_2Mn_{1-y}Fe_yP_2O_7$ series samples (y = 0, 0.2, 0.5, 0.8, and 1); (b) Rietveld refinement of the $Li_2MnP_2O_7$ XRD data.

Table 1. Structural Parameters of the $Li_2Mn_{1-y}Fe_yP_2O_7$ Materials

sample name	a (A)	b (A)	c (A)	β (deg)	volume (A^3)	R_p (%)
single crystal[a]	9.9158	9.8289	11.1800	102.466	1063.9	3.63
$Li_2MnP_2O_7$	9.8941(6)	9.8111(1)	11.1597(8)	102.482	1057.705	8.86
$Li_2Mn_{0.8}Fe_{0.2}P_2O_7$	9.8879(4)	9.8129(4)	11.1368(2)	102.348	1055.608	7.71
$Li_2Mn_{0.5}Fe_{0.5}P_2O_7$	9.8768(2)	9.8085(1)	11.1038(0)	102.111	1051.759	7.87
$Li_2Mn_{0.2}Fe_{0.8}P_2O_7$	9.8712(7)	9.8124(6)	11.0898(2)	101.799	1051.480	7.35
$Li_2Mn_{0.1}Fe_{0.9}P_2O_7$	9.8267(5)	9.7693(5)	11.0389(3)	101.681	1037.801	5.58
$Li_2FeP_2O_7$	9.7997(5)	9.7488(8)	11.0123(6)	101.516	1030.907	6.63
$Li_2Mn_{0.5}Fe_{0.5}P_2O_7$[b]	9.8557(1)	9.7885(4)	11.0806(1)	102.122	1045.144	7.78
$Li_2FeP_2O_7$[b]	9.7993(6)	9.7551(5)	11.0148(7)	101.491	1031.852	4.9

[a] Data taken from ref 19. [b] Synchrotron X-ray diffraction data from Argonne National Laboratory.

energy, according to a Ewald summation, were picked up for further ab initio total energy computations.[33] The voltage profile is obtained directly from this set of ab initio total energy computations.[34]

Results and Discussion

The XRD patterns of all the $Li_2M_{1-y}Fe_yP_2O_7$ compounds (shown in Figure 2a) are similar, indicating the retention of the $Li_2MnP_2O_7$ structure and the existence of a solid solution. However, the prominent peaks are shifted toward higher 2θ values with increasing Fe content, indicating a decrease in the unit cell size, which can be attributed to the smaller ionic radii of Fe^{2+}, in comparison to Mn^{2+}. The GSAS refinement of a $Li_2MnP_2O_7$ sample synthesized at 600 °C is shown in Figure 2b, and the output of the refinement results is summarized in Table 1 for the entire series of compositions. The $Li_2MnP_2O_7$ phase has cell parameters very close to those reported earlier for the $Li_2MnP_2O_7$ single crystal with cell parameters of a = 9.9158(6) Å, b = 9.8289(6) Å, c = 11.180(7) Å, β = 102.466(5)°, volume = 1063.9(7) Å^3.[19] Furthermore, we could clearly observe that all our materials ($Li_2M_{1-y}Fe_yP_2O_7$, with y = 0, 0.2, 0.5, 0.8, and 1) nucleate in the monoclinic crystal system (space group $P2_1/a$) with the transition-metal centers occupying two crystallographically independent 4*e* sites: one octahedral and the second being square pyramidal. As shown in Table 1 and Figure 3, the unit-cell parameters a and c are reduced gradually with increasing Fe content up to 80%; however, little change is observed for lattice parameter b. However, above 80%, substitution of Fe at the Mn site (square pyramidal 4*e* site) leads to a sharp change in the unit-cell parameters, as well as in the cell volume (Figure 3). Although the XRD patterns for the entire series appear similar, there is a clearer splitting of the [222] and [23$\bar{1}$] peaks as y goes from 0 to 1. For the pure iron compound, the FeO_6 octahedron becomes more symmetric and the Fe−O bonds slightly shorter. In addition, the Rietveld analysis of the synchrotron data suggests the presence of some iron on the lithium site, and this is probably the reason for the reduction in the lattice parameters; no transition metal was observed on the lithium site for the 50% manganese−iron composition.

To confirm the structure at higher Fe concentrations (y = 0.5 and 1.0), we acquired high-energy synchrotron (λ = 0.413612 Å) XRD data and analyzed the crystallographic phase using Rietveld refinement (Figure 4). The results clearly support the belief that (1) even at 100% Fe substitution, the structure remains stable and (2) the novel iron phase crystallizes in the same space group, $P2_1/a$ (see Table 1). For y = 0.5, the R-factors for the Rietveld refinement of the synchrotron diffraction data are the lowest if Fe is allowed to occupy both the octahedral and square pyramidal sites randomly.

We investigated the structural stability, as well as the oxidation states, of Fe and Mn by heating the materials in oxygen using a TGA (see Figure 5a). The weight gains observed were consistent with oxidation of all the ferrous ions to ferric ions, and no oxidation of the manganese as expected from the relative oxidation state stabilities

(33) Toukmaji, A.; Board, J. A. *Comput. Phys. Commun.* **1996**, *95*, 73.
(34) Aydinol, M.; Kohan, A.; Ceder, G.; Cho, K.; Joannopoulos, J. *Phys. Rev. B* **1997**, *56*, 1354.

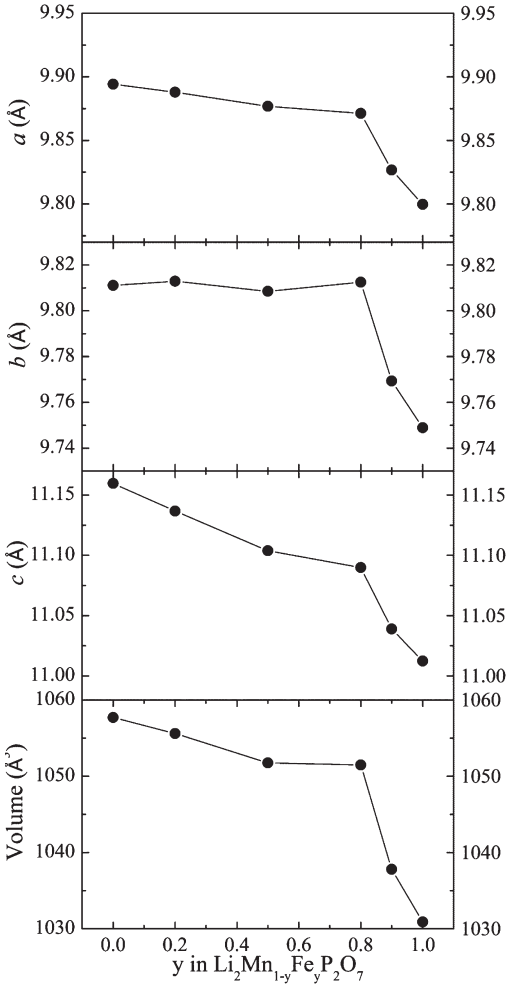

Figure 3. Lattice parameters of $Li_2Mn_{1-y}Fe_yP_2O_7$, as a function of the iron content.

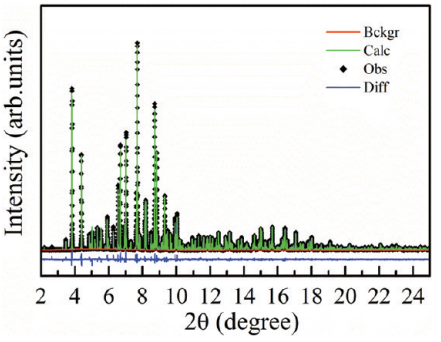

Figure 4. Synchrotron powder XRD pattern (λ = 0.413612 Å) of $Li_2FeP_2O_7$; the experimental data (diamond dots, ◆), calculated pattern (green line), and difference curve (blue line) are clearly indicated.

at 600 °C: $Mn^{2+} > Mn^{3+}$ and $Fe^{3+} > Fe^{2+}$.[35] The weight gain also indicated that all of the iron is in the ferrous state. The oxidation products obtained after oxidation were determined by XRD. The results are shown in Figure 5b, and they indicate the presence of $Li_2MnP_2O_7$, $LiFeP_2O_7$, $L_4P_2O_7$, and Fe_2O_3. This is consistent with the following reaction:

$$12Li_2FeP_2O_7 + 3O_2 \rightarrow 8LiFeP_2O_7 + 4Li_4P_2O_7 + 2Fe_2O_3$$

(35) Whittingham, M. S.; Song, Y.; Lutta, S.; Zavalij, P. Y.; Chernova, N. A. *J. Mater. Chem.* **2005**, *15*, 3362.

Although it has been reported that "wet" methods generally result in smaller particles and higher-surface-area products than solid-state reaction,[36] the particle size of our samples is not very small (see Figure 6). The average particle size is on the order of 5−10 μm, independent of the Fe content. The shapes of the particles are somewhat irregular; nevertheless, with increasing Fe content, the particle size becomes much more uniform, without many agglomerated large particles. An EDS (energy-dispersive spectroscopy) analysis was consistent with the expected Mn:Fe ratio.

We investigated the magnetic properties of $Li_2Mn_{1-y}Fe_yP_2O_7$ to determine the oxidation states of the transition metals and characterize any magnetic interactions that may be present. Curie−Weiss paramagnetic behavior is observed for all the compositions above 50 K, as indicated by the linear dependences of the reciprocal susceptibilities (see Figure 7). The fit of the reciprocal susceptibilities to the Curie−Weiss law, $\chi = \chi_0 + C_M/(T - \Theta)$ (where χ_0 is the temperature-independent contribution, C_M is the molar Curie constant associated with the effective magnetic moment, $\mu = (8C_M)^{1/2}$, and Θ is the Curie−Weiss temperature) results in the parameters presented in Table 2. The temperature-independent contributions are diamagnetic for $Li_2MnP_2O_7$ and turn paramagnetic for the Fe-containing compounds. The latter agrees well with the positive temperature-independent contribution reported for $LiFePO_4$.[37]

The irregular variations in the values of χ_0 possibly indicate some magnetic impurities, such as iron oxides and phosphides, present in the reaction product in amounts below the sensitivity of the XRD analysis. The Θ values change from negative to positive as the Fe content increases, indicating that the dominating magnetic exchange switches from antiferromagnetic in $Li_2MnP_2O_7$ to ferromagnetic in $Li_2FeP_2O_7$. The absolute Θ values are small, which reflects weak magnetic exchange. The effective magnetic moment decreases with increasing Fe content in the series. For $Li_2MnP_2O_7$, $\mu = 5.89\ \mu_B$, in excellent agreement with the value of 5.92 μ_B that is expected for the d^5 Mn^{2+} ion. For $Li_2FeP_2O_7$, μ = 5.17 μ_B, which is very close to the value of 5.20 μ_B that is found for single-crystal $LiFePO_4$ with the same Fe^{2+} oxidation state.[37] The effective magnetic moments for the intermediate compositions can be calculated as $\mu = [y\mu_{Fe}{}^2 + (1 - y)\mu_{Mn}{}^2]^{1/2}$. Since the Fe^{2+} ion has incompletely quenched the orbital contribution, the calculation of the theoretical magnetic moment is nontrivial. Thus, we used the experimental μ_{Fe} value of 5.17 μ_B in this calculation, whereas, for μ_{Mn}, the theoretical value of 5.92 μ_B was used. The magnetic moments so obtained are consistent with the experimental values (Table 2), confirming the 2+ oxidation states for Fe^{2+} and Mn^{2+} throughout the entire series.

At lower temperatures, deviations from the Curie−Weiss behavior are observed. The iron-rich compounds show a sharp increase of the magnetic susceptibility below 10 K, indicative of a magnetic ordering transition

(36) Wurm, C.; Morcrette, M.; Rousse, G.; Dupont, L.; Masquelier, C. *Chem. Mater.* **2002**, *14*, 2701.
(37) Liang, G.; Park, K.; Li, J.; Benson, R. E.; Vaknin, D.; Markert, J. T.; Croft, M. C. *Phys. Rev. B* **2008**, *77*, 064414.

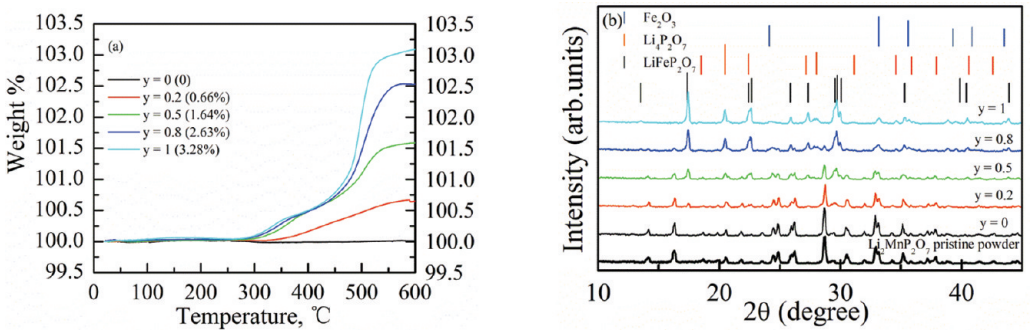

Figure 5. (a) TGA of $Li_2Mn_{1-y}Fe_yP_2O_7$ for $y = 0, 0.2, 0.5, 0.8$, and 1; the calculated weight gain for oxidation of the iron from ferrous to ferric is given in parentheses. (b) XRD patterns of the products after TGA.

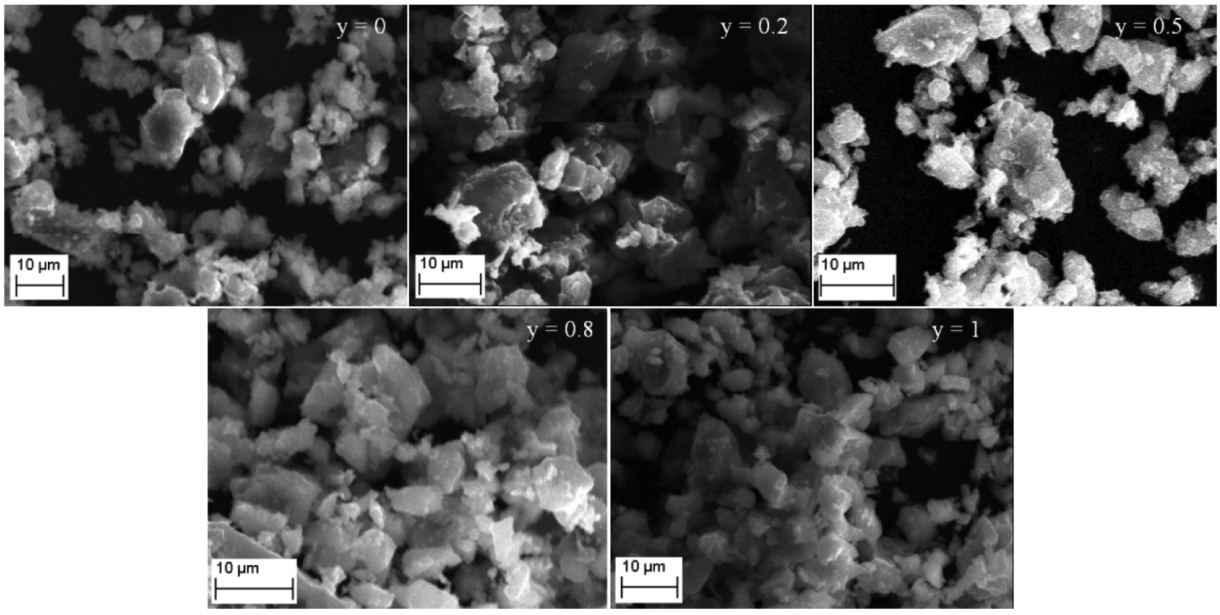

Figure 6. SEM of $Li_2Mn_{1-y}Fe_yP_2O_7$ series samples ($y = 0, 0.2, 0.5, 0.8$, and 1).

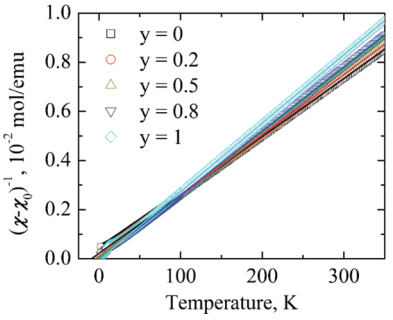

Figure 7. Temperature dependences of $Li_2Mn_{1-y}Fe_yP_2O_7$ reciprocal magnetic susceptibilities and their fit to the Curie−Weiss law.

Table 2. Magnetic Parameters of $Li_2Mn_{1-y}Fe_yP_2O_7$

y	χ_0 ($\times 10^{-4}$ emu/mol)	C_M (emu K/mol)	Θ (K)	μ (μ_B)	μ_{theor} (μ_B)
1	1.0	3.335	11.5	5.17	5.17
0.8	2.0	3.575	9.7	5.34	5.32
0.5	0.5	3.713	5.2	5.45	5.55
0.2	4.0	4.050	−4.1	5.69	5.77
0	−5.0	4.332	−13.3	5.89	5.92

(see Figure 8a). With increasing Mn content, the transition shifts to a lower temperature and seems to disappear when the Mn content reaches unity. The details of the magnetic ordering can be derived from the field-cooled and zero-field-cooled susceptibilities (see Figure 8). For $Li_2FeP_2O_7$, FC and ZFC curves deviate just below 10 K, with the ZFC curve showing a maximum at 9 K and the FC curve reaching saturation at 5 K. Such behavior is typical of ferrimagnetic ordering, where a small magnetic moment is formed because of either not exactly antiparallel arrangements of spins or slightly different magnetic moments of sublattices in the overall antiferromagnetic spin structure. For $Li_2MnP_2O_7$, the FC-ZFC curves indicate an onset of an ordering transition at 2.5 K. Since the data was obtained down to only 2 K, the exact nature of this transition remains unclear and will be investigated further.

The details of the chemical bonding in the $Li_2Mn_{1-y}Fe_yP_2O_7$ series are presented in the Fourier transform infrared (FTIR) spectra shown in Figure 9. The peaks located at ~750 and 950 cm^{-1} are attributed to the symmetric and antisymmetric P−O−P vibrations that are typical of the pyrophosphate group. The O−P−O bending and P−O stretching vibrational frequencies associated with the PO_4 groups are shown as multiple bands in

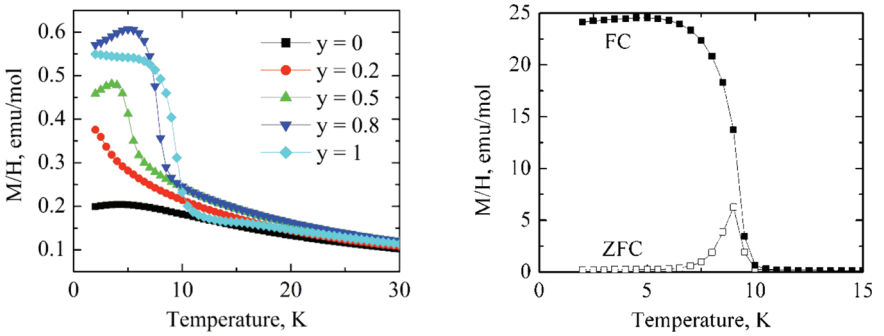

Figure 8. (a) Low-temperature magnetic susceptibility of $Li_2Mn_{1-y}Fe_yP_2O_7$; (b) field-cooled (FC) and zero-field-cooled (ZFC) susceptibilities of $Li_2FeP_2O_7$.

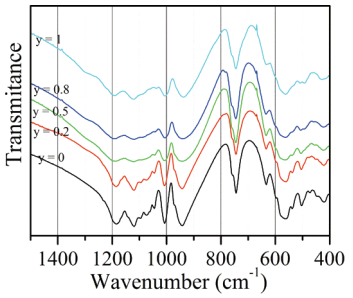

Figure 9. FTIR spectra of the $Li_2Mn_{1-y}Fe_yP_2O_7$ series (y = 0, 0.2, 0.5, 0.8, and 1).

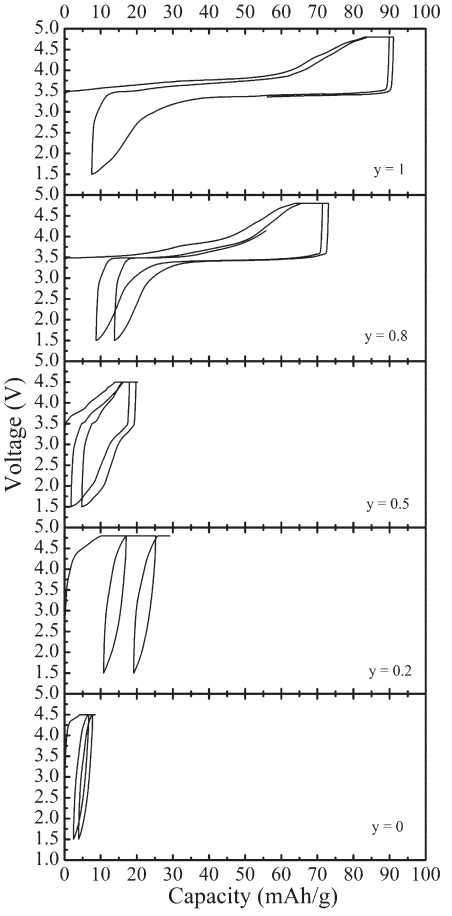

Figure 10. Electrochemical performance of $Li_2Mn_{1-y}Fe_yP_2O_7$ (y = 0, 0.2, 0.5, 0.8, and 1). The current density is 0.1 mA/cm^2.

the ranges of 400−680 cm^{-1} and 1000−1300 cm^{-1}, respectively.[38,39] The similarity of all these vibrational spectra confirms the similar P−O environment in the entire series of samples.

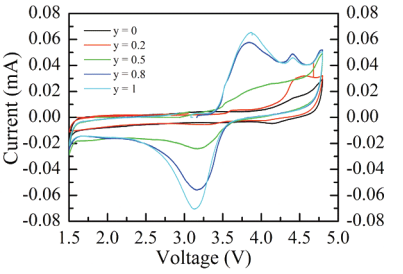

Figure 11. Cyclic voltammetry of $Li_2Mn_{1-y}Fe_yP_2O_7$ (y = 0, 0.2, 0.5, 0.8, and 1) samples at a scanning rate of 0.05 mV/s between 1.5 V and 4.8 V.

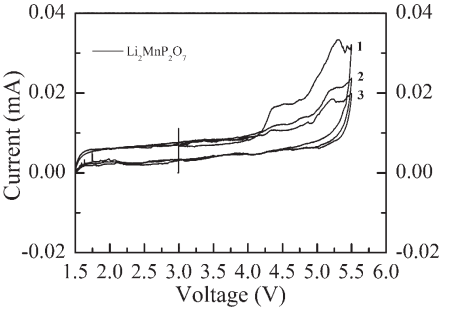

Figure 12. Cyclic voltammetry of a $Li_2MnP_2O_7$ sample at a scanning rate of 0.05 mV/s between 1.5 V and 5.5 V.

The electrochemical behavior of the $Li_2Mn_{1-y}Fe_yP_2O_7$ materials are compared in Figure 10. For the Mn-only phase, the electrochemistry is very poor: it has low capacity, high polarization, and no voltage plateau during charge or discharge. With increasing Fe content, the capacity increases gradually, and the charge/discharge plateaus become more and more apparent, close to 3.5 V. For $Li_2FeP_2O_7$, the discharge plateau appears at ~3.2 V, which is higher than that for $LiFeP_2O_7$ (2.9 V), and the reversible capacity obtained is ~85 mAh/g, which is 77% of the theoretical capacity, assuming that one lithium can be cycled. These data do not show any indication of a second lithium ion being active. Similar to the olivine-structured phosphate compound, the poor conductivity

(38) Huang, Q.; Hwu, S. J. *Inorg. Chem.* **1998**, *37*, 5869.
(39) Bih, H.; Saadoune, I.; Ehrenberg, H.; Fuess, H. *J. Solid State Chem.* **2009**, *182*, 821.

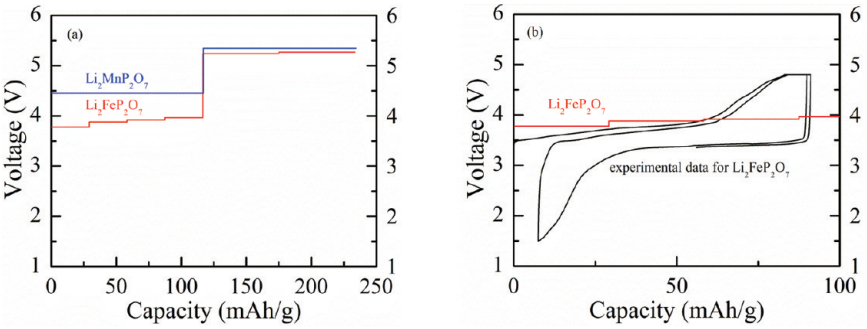

Figure 13. (a) Calculated voltage profiles for $Li_2MnP_2O_7$ and $Li_2FeP_2O_7$ using ab initio computation. (b) Comparison of the calculated and experimental data for $Li_2FeP_2O_7$.

and/or large particle size could be the main factors limiting the capacity. Carbon coating and/or nanosizing may help further improve the capacity. Initial ex situ XRD studies on charged and cycled $Li_2FeP_2O_7$ electrodes show some lattice parameter changes on lithium removal, but the return of the original structure upon subsequent lithium insertion.

To better understand the electrochemical reactions occurring during the charge−discharge process, cyclic voltammograms were acquired (see Figure 11). Almost no peak is seen for the Mn-only $Li_2MnP_2O_7$, which is consistent with its poor electrochemical behavior. For $Li_2Mn_{0.8}Fe_{0.2}P_2O_7$, two small oxidation peaks at ~3.7 V and ~4.5 V appear, which should correspond to Fe^{2+}/Fe^{3+} and Mn^{2+}/Mn^{3+} redox couples, respectively. However, there still is no apparent reduction peak. With further increases of the Fe content to 0.5 ($Li_2Mn_{0.5}Fe_{0.5}P_2O_7$), a very wide oxidation peak, spanning from 3.8 V to 4.2 V, is observed, together with a small reduction peak at ~3.2 V. This is consistent with a very slantwise charging curve and a very short discharging plateau above 3 V for the $y = 0.5$ sample. When the Fe content is above 0.8, the broad oxidation peak is resolved into two peaks, at ~3.8 V and ~4.5 V; the origin of the 4.5 V peak is presently unknown, because it is not predicted from theory, nor is it obtained from electrolyte decomposition. The intensities of the oxidation and reduction peaks for $Li_2FeP_2O_7$ increase significantly, corresponding to the significantly increased capacity, as observed in the cycling performance. Also noticeable is the onset of another peak at ~4.8 V, which may come from the Fe^{3+}/Fe^{4+} redox couple. All these peaks are relatively broad, indicating a solid-solution lithiation/delithiation mechanism, not two-phase behavior. In addition, the marked difference between the oxidation and reduction voltages suggests a large polarization in pyrophosphate samples. To check whether the extraction of the second lithium ion is possible, the cyclic voltammetry for $Li_2MnP_2O_7$ was performed with an extended voltage range of 1.5−5.5 V (see Figure 12). The voltammogram does not appear very smooth, as the electrolyte decomposition might be initiated while cycling beyond the normal potential limit (>4.5 V). We clearly observe another oxidation peak at a much higher potential of ~5.3 V, which might be due to the Mn^{3+}/Mn^{4+} redox couple. However, unlike that for Fe, the corresponding reduction peak for Mn^{4+}/Mn^{3+} is missing. The same holds true for the first oxidation peak at ~4.5 V. This may be caused by the poor conductivity of the material or the decomposition of the electrolyte.

The calculated voltage profiles for the redox processes are presented in Figure 13a. Two voltage plateaus exist during the delithiation of $Li_2MnP_2O_7$ and $Li_2FeP_2O_7$, corresponding to the extraction of the two lithium ions with the oxidation of $Mn^{2+} \rightarrow Mn^{3+} \rightarrow Mn^{4+}$ and $Fe^{2+} \rightarrow Fe^{3+} \rightarrow Fe^{4+}$, respectively. According to this calculation, the oxidation potentials for the Mn^{2+}/Mn^{3+}, Mn^{3+}/Mn^{4+}, Fe^{2+}/Fe^{3+}, and Fe^{3+}/Fe^{4+} redox couples in $Li_2MP_2O_7$ compounds are located at ~4.47, 5.3, 3.8, and 5.2 V, respectively. The experimental and theoretical voltage profiles of $Li_2FeP_2O_7$ are compared directly in Figure 13b. Good agreement is obtained, especially up to 65 mAh/g. The second voltage is so high that we cannot observe it experimentally in the available voltage window. For $Li_2MnP_2O_7$, although no experimental voltage profile is obtained, because of its very poor capacity, good agreement with the cyclic voltammetry is found: two oxidation peaks are observed, at ~4.5 V and ~5.3 V.

Conclusion

Novel pyrophosphate solid solutions with a composition of $Li_2Mn_{1-y}Fe_yP_2O_7$ ($0 \le y \le 1$) were synthesized and characterized structurally and electrochemically as cathode materials for Li-ion batteries. The entire series crystallizes in the monoclinic $P2_1/a$ space group, with lattice parameters that decrease as the iron content increases. Thermogravimetric analysis and magnetic tests confirm the 2+ oxidation state for both Mn and Fe. Lithium-ion extraction and insertion in this pyrophosphate structure is demonstrated, with iron-rich phases showing better performance than manganese-rich ones. The highest capacity obtained for $Li_2FeP_2O_7$ is 85 mAh/g, which is ~77% of that expected for one lithium removal. The cyclic voltammetry, however, reveals second oxidation peaks, at ~5 V and ~5.3 V for $Li_2FeP_2O_7$ and $Li_2MnP_2O_7$, respectively, suggesting that Fe^{3+}/Fe^{4+} and Mn^{3+}/Mn^{4+} redox couples are active. The redox potentials obtained by the ab initio calculations are in perfect agreement with those obtained experimentally. These findings indicate that the second lithium ion could be cycled, if a stable high-voltage electrolyte is found and electronic conductivity is enhanced.

Acknowledgment. The work at Binghamton and MIT was supported by the Assistant Secretary for Energy Efficiency and

Renewable Energy, Office of Vehicle Technologies of the U.S. Department of Energy (under Contract No. DE-AC02-05CH11231), under the Batteries for Advanced Transportation Technologies (BATT) Program (under Subcontract No. 6807148). Use of the Advanced Photon Source at Argonne National Laboratory is supported by the U.S. Department of Energy, Office of Science, Office of Basic Energy Sciences (under Contract No. DE-AC02-06CH11357). This work was first presented at the International Meeting on Lithium Batteries in Montreal, Canada, June 2010.